Fluid Dynamics, Vol. 37, No. 6, 2002, pp. 877–888. Translated from Izvestiya Rossiiskoi Academii Nauk, Mekhanika Zhidkosti i Gaza, No. 6, 2002, pp. 35–47.

Investigation of Different Condensation Regimes in Isobaric Turbulent Air-Steam Jets

A. B. Vatazhin, I. R. Safin, and E. K. Kholshchevnikova

Received April 4, 2002

Abstract — Condensation in axisymmetric turbulent air-steam jets is studied theoretically and experimentally under bench experiment conditions in which a hot mist jet is injected from a nozzle into air. On the basis of the physico-mathematical model developed, four problems are considered: homogeneous condensation in the jet at a fairly low ambient air temperature, heterogeneous condensation on particles introduced into the jet at the nozzle outlet, heterogeneous condensation on particles ejected into the jet from the surrounding space, and condensation on ions entering the jet from a corona point on the flow axis. The local characteristics of the dispersed phase (mean particle size, standard deviation of the particle size, particle number and volume concentrations) and its integral characteristics (coefficient of vapor conversion into condensed phase and the optical thickness of the jet in different sections) are determined.

The calculation results are compared with experimental data. As an application of the model developed, the characteristics of heterogeneous condensation in the jets of certain modern aircraft engines (IL-96-300, Tu-204, MiG-29, Boeing-707) are found on the assumption that the condensation occurs on particles entering the jet at the nozzle outlet and the particle growth rate in all stages (including the initial stage of particle irrigation) coincides with the growth rate of liquid drops.

Keywords: condensation, jet, aircraft engines.

Mathematical modeling of turbulent bench and aircraft engine jets in the presence of condensation has been going on for several decades. The development of a physico-mathematical model of these flows is a complex problem. In general, this model should include the hydrodynamic and kinetic equations, the equations of the turbulence model, the polydisperse phase conservation equations, and in some cases at least an approximate procedure for averaging the source terms.

Among the many publications devoted to this subject, we should mention the study [1] in which the vapor supersaturation in "frozen" turbulent jets was found, the series of studies [2–9] in which homogeneous and heterogeneous condensation in turbulent bench and engine jets was investigated theoretically and numerically, the study [10] in which semi-empirical methods of investigating condensation in turbulent jets were developed, the papers [11, 12] in which the detailed physico-chemical processes in engine jets were examined in the quasi-one-dimensional approximation, and the paper [13] in which homogeneous condensation in a free turbulent jet was considered. Since all the models used (whether relatively simple or more complex) contain many theoretical and semi-empirical submodels, which have their own limits of validity, it is natural to inquire whether these models can be applied to real complex turbulent jet flows with condensation.

In connection with this question we note the following. Nowadays, for solving various problems of fluid and gas mechanics commercial computational packages are widely used. However, the limits of validity of the physical models used in these packages are often unknown to the user. They are made into fetishes, and their physico-mathematical content is gradually forgotten.

In this study we pose the problem of investigating numerically fairly complex condensing jet flows with different boundary conditions. The initial and boundary conditions for the temperature and the velocity are taken to be the same as in experimental studies of bench air-steam jets [3, 4, 14–16]. Using the unique model [6] modified for determining the particle size distribution, we will study turbulent jet flows with

0015–4628/02/3706–0877$27.00

homogeneous condensation at fairly low ambient temperatures, heterogeneous condensation on particles introduced into the jet at the nozzle outlet or ejected from the surrounding space, and condensation on ions introduced into the jet.

Our aim is to model the main trends observed in experiments [3, 4, 14–16] and to obtain new information on the local and global characteristics of the condensed dispersed phase.

We believe this to be the first time that different condensation regimes have been described on the basis of a single physico-mathematical model and the calculation results compared with the experimental data.

1. PHYSICO-MATHEMATICAL MODEL FOR TURBULENT JET FLOWS WITH CONDENSATION

We will consider turbulent isobaric jets with condensation. The medium consists of a carrier gas with components "a" (air), "v" (steam), and "S" (water drops (condensate)). It is assumed that the surfaces of the particles (nucleation centers) introduced into the jet at the nozzle outlet or ejected from the surrounding space immediately become liquid. Accordingly, the particles are treated as drops. The ions introduced into the jet to intensify the condensation are an independent component, whose concentration decreases due to partial conversion of the ions into drop-nuclei and their partial absorption by the surfaces of the drops already formed in the flow. The ion concentration is many orders smaller than that of the neutral particles and hence the contribution of the ions to the total medium density is insignificant.

Since the particles (water drops) are small, their dynamic and thermal relaxation times in the gas flow are also small. Accordingly, the temperature and velocity of the carrier and dispersed phases are assumed to be identical. The ions and the charged drops induce their own electric field. Due to the fairly low concentration of the ions introduced into the flow, the effect of this field may be neglected.

The unknown quantities are the longitudinal and transverse velocity components of the medium u and v, the enthalpy and the stagnation enthalpy h and H, the temperature and the density T and ρ, and the mass concentrations of air, steam, and particles: α_a, α_v, and α_S.

The system of equations for these flows includes the gasdynamic and kinetic equations in the form [2, 6]. The gasdynamic equations are:

$$\frac{\partial \rho u y}{\partial x} + \frac{\partial \rho v y}{\partial y} = 0 \tag{1.1}$$

$$L(u;\ 1) = 0, \quad L(H,\ \mathrm{Pr}) = \frac{1}{y}\frac{\partial}{\partial y}\left[\rho\left(1 - \frac{1}{\mathrm{Pr}}\right)\varepsilon y \frac{\partial u^2/2}{\partial y}\right], \quad L(\alpha_a;\ \mathrm{Sc}) = 0 \tag{1.2}$$

$$L(\xi;\ \Gamma) \equiv \rho u \frac{\partial \xi}{\partial x} + \rho v \frac{\partial \xi}{\partial y} - \frac{1}{y}\frac{\partial}{\partial y}\left(\rho \frac{\varepsilon}{\Gamma} y \frac{\partial \xi}{\partial y}\right), \qquad H = h + \frac{u^2}{2} \tag{1.3}$$

$$h = c_{pa}\alpha_a T + c_{pv}\alpha_v T + c_{pv}\alpha_S T - \alpha_S L^\circ,$$

$$p = p_\infty = \rho T(\alpha_a R_a + \alpha_v R_v), \qquad \alpha_a + \alpha_v + \alpha_S = 1$$

Here, x and y are the longitudinal and transverse coordinates, p is a constant pressure equal to the pressure in the surrounding medium, c_{pi} and $R_i (i = a,\ v)$ are the specific heats and gas constants of the air and the steam, ε is the turbulent viscosity, L° is the specific latent heat of phase transition, and Pr and Sc are the Prandtl and Schmidt numbers, both assumed to be equal to 0.7. The turbulent-viscosity coefficient ε entering into these equations is determined from the turbulence model [17]:

$$L(\varepsilon,\ 0.5) = \alpha^* \rho \varepsilon \left|\frac{du}{dy}\right|, \qquad \alpha^* = 0.2 - \frac{5\varepsilon}{a^2}\left|\frac{\partial u}{\partial y}\right| \tag{1.4}$$

$$a^2 = \frac{p}{\rho}\frac{A}{A - 1}, \qquad A = \frac{\alpha_a c_{pa} + \alpha_v c_{pv}}{\alpha_a R_a + \alpha_v R_v}$$

Here, a is the sonic velocity in the air-steam carrier medium in the absence of condensation.

The kinetic equations are used for determining the value of α_s. The initial equation is the equation for the drop size and charge distribution function f, which is equal to the number of drops of size r and charge Q per unit mass of the medium at a given point in space at a given instant of time [2]:

$$L(f,\ \mathrm{Sc}) = -\frac{\partial}{\partial r}\rho\dot{r}f\ -\ \frac{\partial}{\partial Q}\rho\dot{Q}f\ +\ I_1\delta(r\ -\ r_*)\delta Q\ +\ I_2\delta(r\ -\ r_*)\delta(Q\ -\ e) \tag{1.5}$$

Here, I_1 and I_2 are the rates of homogeneous and "electric" (in the presence of ions) nucleation, $\delta(z)$ is the delta-function of z, r_* and r_{*i} are the critical radii of the drop-nuclei for homogeneous and electric nucleation, $\dot{r}$ and $\dot{Q}$ are the growth rates of the single-drop size and charge, and e is the ion charge. We recall that Eq. (1.5) is obtained from the initial equation for f written for the instantaneous values using the traditional procedure which includes rewriting the equation in terms of the mean and pulsatory components of the quantities, subsequent averaging, approximating the two-point correlations by means of the Boussinesq model, neglecting the triple correlations, using the boundary layer approximation, "quasi-laminar" averaging of the source terms, and making special assumptions concerning the correlations containing the density pulsation. We note that this procedure was used for obtaining Eqs. (1.1)–(1.4).

The kinetic and electrokinetic parameters entering into (1.5) are determined from the formulas:

$$\dot{r} = \dot{r}(r,\ p_v,\ T),\quad \dot{Q} = 4\pi qrD_i,\quad r_* = r_*(p_v,\ T),\quad r_{*i} = r_{*i}(p_v,\ T) \tag{1.6}$$

$$I_1 = I_1(p_v,\ T),\quad I_2 = qG(p_v,\ T),\quad p_v = p_\infty\frac{\alpha_v R_v}{\alpha_a R_a\ +\ \alpha_v R_v}$$

Here, p_v is the partial vapor pressure, q is the ion space charge density, and D_i is the ion diffusion coefficient. The expression for $\dot{r}$ is given in [6, 18, 19]. The formula for $\dot{Q}$ corresponds to diffusion charging of the particle and the assumption that its charge Q is fairly small [20]. The quantities r_* and I_1 are determined on the basis of liquid-drop condensation theory [21], and r_{*i} and I_2 are determined using the results [3, 21–23].

Multiplying Eq. (1.5) by r^kQ^m and integrating over particle size and charge space, we obtain an unclosed system of equations for the moments [2, 6]

$$\Omega_{km} = \int\limits_{(r)}\int\limits_{(Q)} r^kQ^m f\,dr\,dQ \tag{1.7}$$

The equations for Ω_{k0} ($k = 0,\ 1,\ 2,\ 3$) and Ω_{01}, required for the further analysis, take the form [2, 6]:

$$L(\Omega_{k0};\ \mathrm{Sc}) = k\rho\int\limits_{(Q)}\int\limits_{(r)}\dot{r}r^{k-1}f\,dr\,dQ\ +\ Ir_*^k\ +\ I_2r_{*i}^k \tag{1.8}$$

$$L(\Omega_{01},\ \mathrm{Sc}) = 4\pi qD_i\rho\Omega_{10}\ +\ I_2e \tag{1.9}$$

Here and in what follows, it is assumed that the turbulent transport is the same for all the scalar quantities.

The equation for the ion charge density q follows from the following initial conservation equation for the electric current $\mathbf{j}$ written for the instantaneous quantities in the turbulent flow:

$$\mathrm{div}\,\mathbf{j} = 0,\qquad \mathbf{j} = q\mathbf{v}\ +\ \rho\mathbf{v}\Omega_{01} \tag{1.10}$$

The first term in the expression for $\mathbf{j}$ corresponds to the ion current and the second to the charged-drop current.

The analog of Eq. (1.10) written for the mean (in the turbulent flow) quantities and obtained as a result of applying the averaging procedure described above to Eq. (1.10) and using Eq. (1.9) for Ω_{01} takes the form:

$$L(\alpha_i,\ \mathrm{Sc}) = -4\pi\rho^2D_i\alpha_i\Omega_{10}\ -\ I_2m_i;\quad \alpha_i = \frac{\rho_i}{\rho},\quad \rho_i = m_in_i,\quad q = en_i \tag{1.11}$$

Here, α_i is the ion mass concentration, ρ_i and n_i are the ion density and number concentration, and m_i and e are the ion mass and charge, equal to the electron charge.

The following physical quantities can be expressed in terms of the moments introduced:

$$n = \rho\Omega_{00}, \quad \rho_s = \frac{4}{3}\pi\rho_w\rho\Omega_{30}, \quad \alpha_S = \frac{4}{3}\pi\rho_w\Omega_{30}, \quad c = \frac{\rho_S}{\rho_w}, \quad q_S = \rho\Omega_{01} \tag{1.12}$$

$$\mathbf{j} = \frac{e}{m_i}\left(\rho\mathbf{v}\alpha_i - \frac{\rho\varepsilon}{\mathrm{Sc}}\nabla\alpha_i\right) + \rho\mathbf{v}\Omega_{01} - \frac{\rho\varepsilon}{\mathrm{Sc}}\nabla\Omega_{01}$$

Here, n and c are the dispersed-phase number and volume concentrations, ρ_S is the dispersed-phase mass density, q_S is the dispersed-phase space charge density, and ρ_w is the water density.

If the function $f(r,\ Q)$ is known, Eqs. (1.8), (1.9), and (1.11) for Ω_{i0} ($i = 0,\ 1,\ 2,\ 3$), Ω_{01}, and α_i, solved simultaneously with gasdynamic equations (1.1)–(1.4), make it possible to determine the required parameters of the carrier and dispersed phases.

The structure of the integrands in moment equations (1.8)–(1.9) allows us to introduce only the drop size distribution function f°:

$$f^\circ = f^\circ(r) = \int_Q f(r,\ Q)\,dQ$$

In accordance with [24], we will approximate the function f° by a log-normal distribution characterized by three parameters. After substituting the expression for the log-normal function in formulas (1.7) for the moments Ω_{00}, Ω_{i0}, and Ω_{20}, we express these parameters in terms of the moments. The expression for f° takes the form:

$$f^\circ = \frac{\Omega_{00}}{\sqrt{2\pi}\,r\ln\sigma^*}\exp\left[-\frac{(\ln r - \ln r_m)^2}{2\ln^2\sigma^*}\right], \quad r_m^2 = \frac{\omega_{10}^4}{\Omega_{20}\Omega_{00}^3}, \quad \ln^2\sigma^* = \ln\left(\frac{\Omega_{20}\Omega_{00}}{\Omega_{10}^2}\right) \tag{1.13}$$

Using (1.13), the mean drop size $\langle r\rangle$ and the drop-size standard deviation σ^2 can be written as follows:

$$\langle r\rangle = \frac{\Omega_{10}}{\Omega_{00}}, \qquad \sigma^2 = \frac{\Omega_{20}\Omega_{00} - \Omega_{10}^2}{\Omega_{00}^2}$$

Integration of Eqs. (1.1)–(1.4), (1.8), (1.9), (1.11) with the use of approximation (1.13) for f° yields the gas and dispersed-phase parameters as functions of the x and y coordinates in the jet.

On the basis of the physico-mathematical model formulated we performed numerical modeling of turbulent jet flows with condensation under the conditions of experiments [14, 15] in which a hot steam jet with a flow core velocity u_0 and temperature T_0 was injected into the surrounding space filled with air at the temperature T_∞ and constant pressure p_∞. During numerical modeling, we varied the temperature T_∞ and the methods of introducing the nucleation centers into the jet. We considered the regimes of homogeneous condensation, heterogeneous condensation, and condensation on ions introduced into the jet by a corona discharge whose electrode was located on the jet axis. In formulating the boundary conditions at the jet outlet, the dynamic and thermal boundary layers formed on the inner and outer nozzle surfaces were taken into account, the velocity and temperature profiles were taken from experiment. The distribution of the turbulent viscosity ε in the nozzle outlet section, specified in accordance with [25], tended asymptotically to the constant value ε_∞ (at $y = \infty$) for co-current flow. In all the calculations it was assumed that $u_0 = 205$ m/s, $T_0 = 375$ K, $u_\infty = 10$ m/s, $p_\infty = 10^5$ Pa (1 atm), $\alpha_{a0} = 0$, $\alpha_{v0} = 1$, and $\alpha_{v\infty} = 0$.

2. HOMOGENEOUS CONDENSATION

Homogeneous condensation develops at a fairly low temperature of the surrounding medium. In the calculations we assumed that no foreign nucleation centers were introduced into the jet and that the condensation was attributable to the presence of the source term I_1 in Eqs. (1.8). The boundary conditions were:

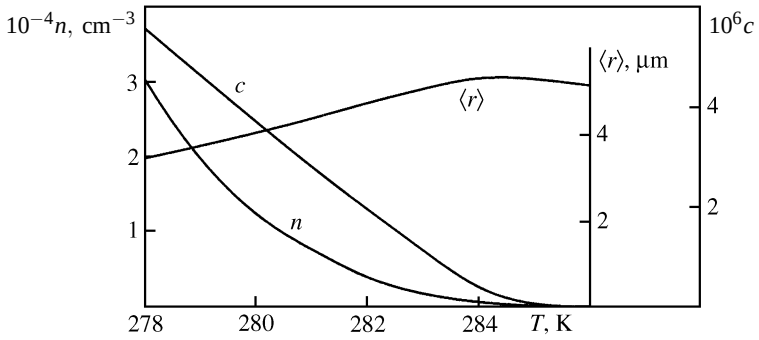

Fig. 1. Dependence of the homogeneous-condensation parameters on the ambient temperature

$$x = 0,\ 0 \le y < \infty: \quad u = u(y),\ H = H(y),\ \varepsilon = \varepsilon(y),\ \Omega_{k0} = 0\ (k = 0,\ 1,\ 2,\ 3),$$
$$\Omega_{01} = 0, \qquad \alpha_i = 0$$
$$x > 0,\ y = \infty: \quad u = u_\infty,\ H = H_\infty,\ \varepsilon = \varepsilon_\infty,\ \Omega_{k0} = 0\ (k = 0,\ 1,\ 2,\ 3),$$
$$\Omega_{01} = 0, \qquad \alpha_i = 0$$

The ambient temperature T_∞ was varied from 278 to 286 K.

Figure 1 shows the particle number and volume concentrations (n and c) and the mean particle radius $\langle r\rangle$ at the point $x = 150y_0$, $y = 0$ as functions of the ambient temperature (y_0 is the nozzle outlet radius). For bench-experiment conditions, the ambient-temperature variation range for which homogeneous condensation is possible extends over only seven degrees. This is confirmed by bench experiments in which the homogeneous-condensation regime was attained only when the room was specially cooled. With increase in the ambient temperature, the nucleation rate decreases, the number of condensation centers declines, and the drop number and volume concentrations fall. In this process, due to the only slight decrease in the vapor pressure for such weak condensation, a larger amount of water accumulates on the nuclei formed and hence the drop radius increases.

Figure 2 (*a* and *b*) shows the distribution of the following parameters along the jet axis ($T_\infty = 278$ K): the supersaturation $S = p_v/p_e$, where $p_e(T)$ is the equilibrium vapor pressure corresponding to $S = 1$; the drop number, volume, and mass concentrations n, c, and α_S; and the drop mean radius and standard deviation $\langle r\rangle$ and σ. Here and in what follows, the longitudinal coordinate is scaled to the nozzle radius. With jet expansion, the temperature of the air-steam mixture in the jet decreases and at $x \approx 20y_0$ conditions are such that the supersaturation attains a maximum. Near this section the nucleation rate I_1 also attains a maximum. Because of this, the drop number concentration n sharply increases and then S, I_1, and n decrease. The decrease in S is connected not only with the ratio of the temperatures in the jet and the surrounding medium but with the condensation process itself, since with increase in the condensate mass the partial vapor pressure decreases. The drop volume and mass concentrations also pass through a maximum, shifted slightly away from the maximum of S. The further decrease of c and α_S is related with jet expansion. The mean drop radius grows steadily, and the standard deviation σ is almost constant and comprises $\approx 10\%$ of the mean radius.

3. HETEROGENEOUS CONDENSATION

Heterogeneous condensation on foreign nuclei can occur at a higher ambient temperature than homogeneous condensation. We will consider condensation when the particles are introduced through the nozzle. The calculations were performed for $T_\infty = 290$ K, $n_0 = 10^6$ cm^{-3}, $r_0 = 0.1$ μm (the subscript "0" denotes the particle parameters at the nozzle outlet). The boundary conditions for the moments are:

$$x = 0,\ 0 \le y \le y_0: \quad \Omega_{k0} = (n_0/\rho_0)r_0^k\ \ (k = 0,\ 1,\ 2,\ 3),\ \ \Omega_{01} = 0,\ \ \alpha_i = 0$$

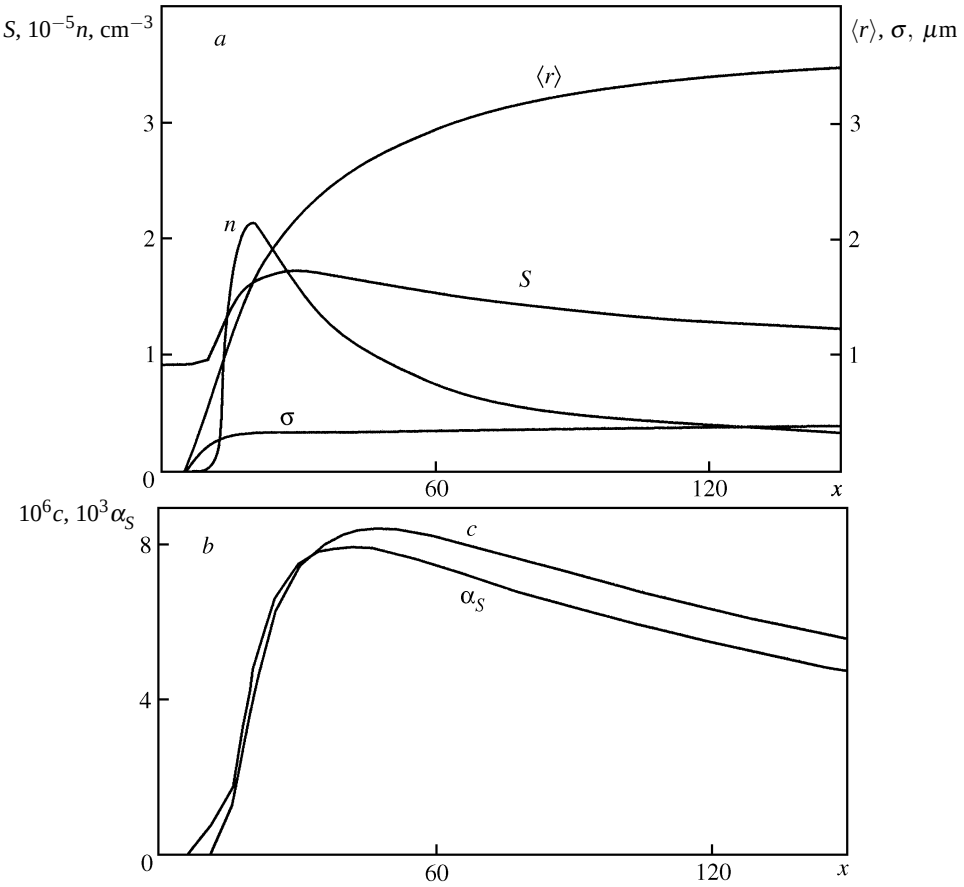

Fig. 2. Variation of the condensation parameters along the jet axis for $T_\infty = 278$ K

$$x > 0,\ \ y = \infty: \quad \Omega_{k0} = 0\ \ (k = 0,\ 1,\ 2,\ 3),\ \ \Omega_{01} = 0,\ \ \alpha_i = 0$$

The calculations performed showed that the dispersed-phase number concentration on the jet axis monotonously decreases with length while the other condensation parameters vary qualitatively in the same way as for homogeneous condensation (Fig. 2).

We will now consider the case when the particles enter the jet from the surrounding space. In experiments [4], the particles were introduced on the jet periphery using the smoke from a cigarette brought close to the jet. The temperature in the outer part of the jet was so chosen that homogeneous condensation did not develop. The introduction of the dust particles resulted in the development of heterogeneous condensation in the jet. For the approximate modeling of this situation, we will consider the problem of the symmetric introduction of particles on the jet periphery over the interval from $x_1 = 10y_0$ to $x_2 = 50y_0$. To avoid errors in the numerical calculation, performed using a marching scheme (all the differential equations except the continuity equation are parabolic), the concentration of the particles introduced was "smeared" over the x coordinate using an exponential function sharply increasing from zero to a given constant value in a small left neighborhood of the point $x = x_1$ and sharply decreasing in the same manner from this value to zero in a small right neighborhood of the point $x = x_2$. Accordingly, the boundary conditions for the moments on the outer jet edge ($y = \infty$) took the form:

$$\Omega_{k0} = (n_\infty/\rho_\infty) r_\infty^k \exp(-x_*^2), \qquad x_* = x - x_1, \qquad x \le x_1$$
$$\Omega_{k0} = (n_\infty/\rho_\infty) r_\infty^k, \qquad x_1 < x < x_2$$
$$\Omega_{k0} = (n_\infty/\rho_\infty) r_\infty^k \exp(-x_*^2), \qquad x_* = x - x_2, \qquad x \ge x_2$$

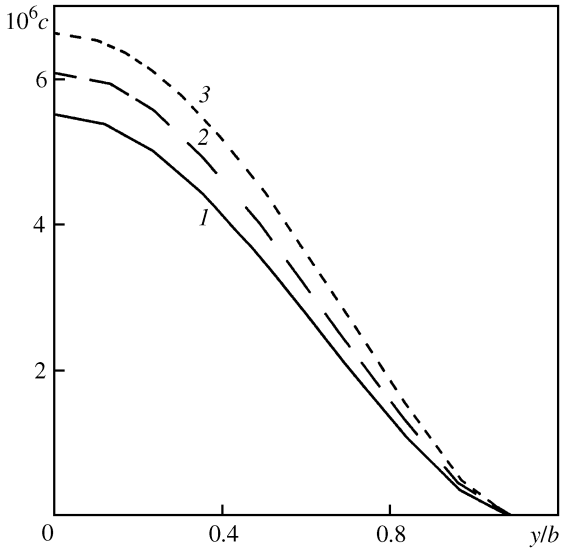

Fig. 3. Drop volume concentration profiles for $x = 150y_0$, $T_\infty = 278$ K: *1* — homogeneous condensation; *2* — simultaneous homogeneous and heterogeneous condensation on particles introduced through the nozzle; *3* — simultaneous homogeneous and heterogeneous condensation on particles introduced from the surrounding space

The particle concentration and radius were taken equal to: $n_\infty = 10^6$ cm^{-3} and $r_\infty = 0.1$ μm. As in the case of particle introduction through the nozzle, the ambient temperature was $T_\infty = 290$ K. The calculations showed that the distributions of the drop volume and mass concentration along the jet axis have maxima at $x \approx 44y_0$ and the drop number concentration n increases monotonously with the jet length since the particles enter the jet over a fairly long interval and at the end of the calculation domain are still reaching the jet axis due to diffusion. The mean drop radius at $x = 150y_0$ is 0.4 μm. In the heterogeneous-condensation regime in question, the mass flow of the drops (irrigated particles) should remain constant in any jet section to the right of the particle introduction region. In the calculations, this mass flow was constant to within 2%.

To compare the homogeneous and heterogeneous condensation regimes, we calculated jet flows in which the particles were introduced through the nozzle and on the jet periphery at $T_\infty = 278$ K. Figure 3 shows the drop volume concentration profiles in the section $x = 150y_0$ (b is the jet half-width) for all the cases considered. Due to diffusion, at a sufficient distance from the nozzle outlet the concentration maximum is located on the jet axis. Near the jet outlet, this maximum lies in the peripheral mixing layer. When foreign particles are introduced into the jet, the drop volume fraction increases. The greater the mass flow of the particles introduced, the greater this increase: curve *3* corresponding to particle introduction on the jet periphery (particle mass flow 0.0716 g/s) lies above curve *2* corresponding to particle introduction through the nozzle (particle mass flow 0.0626 g/s) and curves *2* and *3* lie above curve *1* corresponding to homogeneous condensation (particle mass flow 0.0552 g/s). A similar effect was observed in experiments [4]. (We assume that in this situation the particle mass flow plays the decisive role, rather than the method of particle introduction into the jet.)

4. CONDENSATION ON IONS INTRODUCED INTO THE JET FROM A DISCHARGE POINT

In experiments [4], the discharge point was located on the axis of an air-steam jet at a distance of $16.4y_0$ from the nozzle outlet. When a potential greater than the corona discharge potential is supplied to the discharge point, an electric current flows and outside a very narrow ionization zone the charge carriers are ions. Under certain temperature conditions in the jet, "electric" condensation develops on some of these ions. This experimental situation was modeled by specifying the ion concentration profile n_i in the same section as in the experiment. This profile has a maximum on the jet axis and the quantity n_i decreases sharply

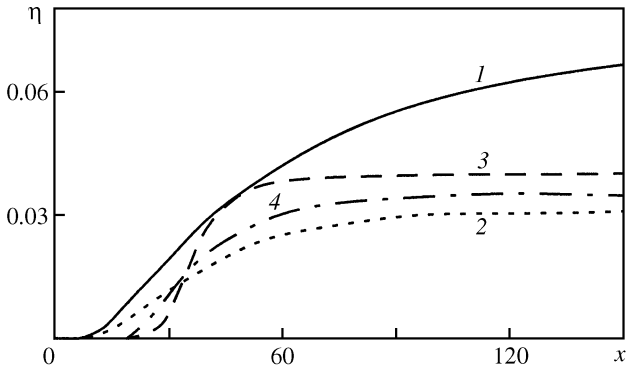

Fig. 4. Variation of the steam conversion rate along the jet axis for different condensation types: *1* — homogeneous condensation, $T_\infty = 278$ K; *2* — heterogeneous condensation on particles introduced through the nozzle; *3* — heterogeneous condensation on particles introduced from the surrounding space; *4* — condensation on ions from a corona discharge point; *2, 3, 4* — $T_\infty = 290$ K

towards the periphery. The profile n_i used in the calculations is described by the function

$$n_i = \varphi(y) = n_{i0}\exp(-(ay)^2)$$

Here the coefficient a was determined from the condition $\varphi = n_{i0}/2$ for $y = 0.5y_i$, where y_i is the effective boundary of the ion jet in its initial section. In the calculations it was assumed that $y_i = 2$ mm, $n_{i0} = 1.13 \times 10^8$ cm^{-3}, $T_\infty = 290$ K, $\alpha_i = n_i m_i/\rho$ (here, by assumption, m_i is the mass of the ion formed from the oxygen molecule.) In the calculations for condensation on ions, Eqs. (1.9) and (1.11) were incorporated into the general system of equations. In the conditions mentioned above, the electric-nucleation rate I_2 was sufficiently high to ensure the development of condensation in the jet. In the absence of ions, there is almost no condensation in the jet.

The calculations showed that, when ions are introduced into the jet, the variation of the condensation characteristics along the jet length (to the right of the ion introduction section) is qualitatively similar to that for homogeneous condensation (Fig. 2). The quantitative data are somewhat different.

Figure 4 shows the variation of the steam-to-condensate conversion rate η with length for the different condensation regimes considered. The quantity $\eta(x)$, equal to the ratio of the drop mass flow to the steam mass flow at the nozzle outlet, is given by the formula

$$\eta = \frac{G_s}{G_{v0}}, \qquad G_s = 2\pi \int\limits_{(r)} \rho_S u y\, dy, \qquad G_{v0} = \pi y_0^2 \rho_{v0} u_0$$

For the given conditions, the steam-to-condensate conversion rate is maximum for homogeneous condensation.

In Fig. 5, the continuous curves show the isolines of the volume concentration c, the triangles show the turbulent-jet gasdynamic boundary, and the circles bound the "visible-condensation" zone obtained in experiments [4] by flow visualization in the laser knife-edge plane. The ions are introduced at $x = 16.4$. The "visible-zone" boundary approximately coincides with the calculated isoline $c \cong 1.5 \cdot 10^{-6}$. Significantly, in the experiments the value $c \approx 10^{-6}$ corresponds approximately to the condensation "visibility" threshold: for $c < 10^{-6}$ the condensation is only slightly visible and, for $c > 10^{-6}$, the condensation is well visible. At the end of the calculation domain, the mean drop radius is 2 μm. This also agrees with experiment [4].

We note that, in the region where S tends to its equilibrium value (after passing through a maximum), the values of the mean drop radius obtained in both experiment [4] and the numerical modeling increase with decrease in the drop number concentration (for homogeneous condensation, heterogeneous condensation with particle introduction through the nozzle, and for condensation on ions) and decrease with increase in the drop concentration (when the particles are introduced on the jet periphery). For equilibrium condensation in

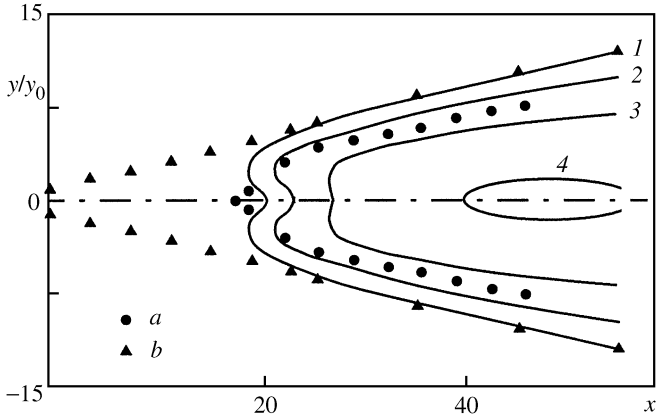

Fig. 5. Volume fraction isolines for the introductions of ions from a corona discharge point, $T_\infty = 290$ K: *a* — visible-zone boundary (experiment); the values of *c* on the isolines are: *1* — 10^{-7}, *2* — 10^{-6}, *3* — 3×10^{-6}, *4* — 6×10^{-6}

the jet, the quantity $c \sim n\langle r\rangle^3$ varies only slightly [4], and the tendency of "inverse proportionality" between $\langle r\rangle$ and n remains valid over the entire region mentioned above. This is also confirmed by the data presented in Fig. 2.

The examples considered above show that the theoretical and numerical model used makes it possible to calculate all the condensation regimes observed experimentally and that the results obtained agree qualitatively with the experimental data. The technique developed is used below for the approximate analysis of condensation in aircraft engine jets.

5. HETEROGENEOUS CONDENSATION IN AIRCRAFT ENGINE JETS

The visible condensation wake behind aircraft is formed at flight altitudes of 9–11 km. Previous calculations (for example, see [9]) demonstrated that, in aircraft jets, only heterogeneous condensation on microparticles (carbon black particles) entering the jet from the engine duct is basically possible. Different mechanisms of water vapor and sulfate condensation on carbon black particles with a broken surface and an electric charge, reacting with a surrounding gas mixture containing positive and negative ions, are now being studied intensively. However, for preliminary estimates it is instructive to use the simple model in which only water vapor is condensed on the microparticles and these particles are supplied with water in the same way as spherical liquid drops.

The calculation results presented below correspond to the case of heterogeneous condensation on monodisperse 0.1 μm particles with the concentration $n_0 = 10^6$ cm^{-3} introduced into the jet through the nozzle outlet. Several kinds of aircraft engines were considered: a single-flow turbojet engine (TJE) and double-flow engines, e.g. a typical engine of the fourth generation (TJEA), a PS-90A engine, and a Boeing-707 engine. The gas from the first and second ducts of the PS-90A and the fourth-generation engine enters a mixing chamber and then the common exhaust duct. The Boeing-707 engine has separate exhaust ducts (at the nozzle outlet the gas streams from the different ducts do not intermix). All the engine data correspond to cruising flight at an altitude of 11 km. For the single-flow engine and Boeing-707 engines, the design flow regimes are considered. The other engines are double-flow with a supersonic nozzle flow operating in the overexpansion regime.

To simplify the calculation of the gasdynamic flow in the exhaust jet in the overexpansion regime, using the one-dimensional theory we determined the parameters in the full flow expansion section (in the isobaric section in which the pressure is equal to the ambient pressure), which was taken to coincide with the nozzle outlet. (For the design flow, the isobaric section exactly coincides with the nozzle outlet). In Table 1, we present the temperature T_e and the Mach number M_e in the isobaric section, the ratio of the co-current jet velocities m, the mist concentration at the nozzle outlet α_{v0}, and the parameters characterizing the condensation on the exhaust jet axis at $x = 500y_0$. (For the Boeing-707 engine, the value of α_{v0} corresponds to the

Table 1

Parameters	Engine type			
	TJE	TJEA	PS-90A	Boeing-707 duct I
T_e, K	564	490	281	605
M_e	0.5	1.38	1.29	≈ 1
m	0.450	0.407	0.562	0.632
α_{v0}	0.0233	0.012	0.004	0.021
S	1.01	1	0.75	1.03
α_S	$0.225 \cdot 10^{-3}$	$0.197 \cdot 10^{-3}$	$0.579 \cdot 10^{-4}$	$0.283 \cdot 10^{-4}$
c	$0.645 \cdot 10^{-7}$	$0.202 \cdot 10^{-6}$	$0.208 \cdot 10^{-7}$	$0.753 \cdot 10^{-8}$
$\langle r \rangle$, μm	0.571	0.905	0.427	0.190
n	$6.05 \cdot 10^4$	$5.09 \cdot 10^4$	$5.17 \cdot 10^4$	$2.14 \cdot 10^5$
η	0.399	0.677	0.351	0.0487
τ	0.769	0.947	0.489	0.242
I_0/I	2.16	2.58	1.63	1.27

first duct and instead of m we present the ratio of the velocities in the second and first ducts in the duct outlet sections).

In addition to the parameters mentioned above, in Table 1 we also present the values of the optical jet thickness τ and the ratio I_0/I related with this thickness and characterizing the decrease in the intensity of radiation directed at right angles to the jet axis after passage through the jet. The optical jet thickness is determined as follows:

$$\tau = \ln(I_0/I) = \int_l n(s) \int_0^\infty \pi r^2 q_{ext}(r) f^*(r,\, s)\, dr\, ds, \qquad n = \rho \Omega_{00}$$

Here, s is a linear coordinate measured along the chosen optical path l (jet diameter), $n(s)$ is the particle concentration, $f^*(r;\, s)$ is the drop size distribution function $f^0(r)$ (see (1.13)) scaled to Ω_{00} and q_{ext} is the extinction coefficient, which for simplicity was approximated by a piecewise-constant function: $q_{ext} = 0$ for $r \le 0.12$ μm and $q_{ext} = 2$ for $r > 0.12$ μm. The parameters τ and I_0/I are used in investigating the atmospheric composition by optical methods. In particular, this is necessary for studying the unfavorable effects of aviation on the environment.

In the calculations, it is necessary to specify the initial profiles of the gasdynamic and kinetic parameters at the nozzle outlet. We assumed that at the nozzle outlet (for the single-flow engine and the double-flow engine with a common exhaust), in each duct outlet section (for the double-flow engine with separate exhausts), and in the surrounding space the parameters mentioned above are constant everywhere, except near the nozzle edge (inner and outer boundary layers). In these zones, the parameters at the nozzle outlet go smoothly over into the outer-flow parameters. In calculating the Boeing-707 engine, the presence of two (external and internal) surfaces, each having its own boundary layer, was taken into account.

For a given temperature regime in the surrounding space, the condensation intensity in the engine jets is mainly affected by the parameters T_e and α_{v0}. The condensation is enhanced with decrease in the exhaust jet temperature (see [14]) and with increase in the steam content in the exhaust jets. The combination of these parameters results in the condensation being most intense and weakest in the TJEA engine and the Boeing-707 engine, respectively.

We note once again that the model used does not take into account any condensation process other than

steam condensation. The results could change if the more detailed physico-chemical processes in engine jets are taken into account. However, the data obtained may be used for a comparative analysis of the integral characteristics of the condensation in the exhaust jets of the engines considered.

Summary. Our numerical modeling demonstrates that, for all the condensation types considered, the supersaturation S and the drop mass and volume concentrations α_s and c vary along the jet axis in a similar way: S, α_S, and c pass through a maximum, S then tends to its equilibrium value, equal to unity, and far from the nozzle α_S and c decrease due to jet expansion. The introduction of particles into a jet with homogeneous condensation intensifies the condensation. The calculation results agree qualitatively with the known experimental data.

REFERENCES

1. A. G. Amelin, *Fundamentals of Mist Formation in Steam Condensation* [in Russian], Khimiya, Moscow (1972).
2. A. B. Vatazhin, "Electrogasdynamic turbulent flows," *Trudy Matem. Inst. AN SSSR*, **186**, 168–176 (1989).
3. *Turbulent Jet Flows with Condensation and Electrophysical Effects (Ed. A. B. Vatazhin)* [in Russian], *Trudy TsIAM*, **1**, No. 1288 (1991).
4. A. Vatazhin, A. Lebedev, V. Likhter, V. Shul'gin, and A. Sorokin, "Turbulent air-steam jets with a condensed dispersed phase: Theory, experiment, numerical modeling," *J. Aerosol. Sci.*, **26**, No. 1, 71–93 (1995).
5. A. B. Vatazhin and A. A. Sorokin, "Atmospheric aerosols of aviation origin and the ecological problems," *Izv. Ross. Akad. Nauk, Mekh. Zhidk. Gaza*, No. 6, 57–72 (1992).
6. A. V. Akimov, A. B. Vatazhin, V. A. Likhter, and A. A. Sorokin, "Steam-air flow in the presence of condensation on ions and electrokinetic processes," *Izv. Ross. Akad. Nauk, Mekh. Zhidk. Gaza*, No. 1, 67–77 (1996).
7. A. B. Vatazhin, A. B. Lebedev, and V. A. Markeev, "Mathematical modeling of different condensation regimes in turbulent isobaric jets," *Izv. Akad. Nauk SSSR, Mekh. Zhidk. Gaza*, No. 1, 67–77 (1985).
8. A. B. Vatazhin, A. Yu. Klimenko, A. B. Lebedev, and A. A. Sorokin, "Homogeneous condensation in submerged turbulent isobaric jets", *Izv. Akad. Nauk SSSR, Mekh. Zhidk. Gaza*, No. 2, 43–52 (1988).
9. A. A. Sorokin and A. B. Lebedev, "Modeling of water aerosol emission in an exhaust jet of a subsonic aircraft and an estimate of the influence of aviation on the aerosol balance in the lower stratosphere," *Preprint TsIAM*, No. 18 (1994).
10. A. L. Stasenko, "Towards a theory of nitrogen oxide chemisorption by water drops in a stratospheric-aircraft jet," *Preprint TsAGI*, No. 51 (1991).
11. A. B. Lebedev, A. M. Starik, and N. S. Titova, "Numerical modeling of non-equilibrium photochemical processes in a subsonic-aircraft wake," *Teplofiz. Vys. Temper.*, **36**, No. 1, 79–93 (1998).
12. A. M. Savel'ev and A. M. Starik, "Dynamics of the formation of sulfate aerosols in jet engine jets," *Izv. Ross. Akad. Nauk, Mekh. Zhidk. Gaza*, No. 1, 108–117 (2001).
13. T. K. Lesniewskii and S. K. Friedlander, "Particle nucleation and growth in a free turbulent jet," *Proc. Roy. Soc. London. Ser. A*, **454**, No. 1977, 2477–2504 (1998).
14. A. B. Vatazhin, V. A. Likhter, and V. I. Shul'gin, "Turbulent condensation jets and the possibility of controlling them by an electric field," in: *Problems of Modern Mechanics. V1. (Ed. L. I. Sedov)*, MSU, Moscow (1983), pp. 113–122.
15. A. B. Vatazhin, R. S. Valeev, V. A. Likhter, V. I. Shul'gin, and V. I. Yagodkin, "Investigation of turbulent air-steam jets in the presence of condensation and the introduction of foreign particles into the flow," *Izv. Akad. Nauk SSSR, Mekh. Zhidk. Gaza*, No. 3, 53–61 (1984).
16. A. B. Vatazhin, V. A. Likhter, A. A. Sorokin, and V. I. Shul'gin, "Corona discharge in an air-steam jet with condensation. Steady-state and pulsatory characteristics," *Trudy TsIAM*, No. 1288 (1991).
17. V. E. Kozlov, A. N. Sekundov, and I. P. Smirnova, "Turbulence models for describing compressible-gas jet flow," *Izv. Akad. Nauk SSSR, Mekh. Zhidk. Gaza*, No. 6, 38–44 (1986).
18. N. A. Fuks, *Mechanics of Aerosols* [in Russian], AS USSR, Moscow (1955).
19. L. E. Sternin, *Fundamentals of Gasdynamics of Two-Phase Nozzle Flows* [in Russian], Mashinostroenie, Moscow (1974).
20. I. P. Vereshchagin, V. I. Levitov, G. Z. Mirzabekyan, and M. M. Pashin, *Fundamentals of Electrogasdynamics of Disperse Systems* [in Russian], Energiya, Moscow (1974).

21. Ya. I. Frenkel', *Kinetic Theory of Liquids* [in Russian], Nauka, Leningrad (1975).
22. Ya. B. Zel'dovich, "A contribution to the new-shape formation theory. Cavitation," *Zh. Experim. Tekh. Fiz.*, **12**, No. 11/12, 525–538 (1942).
23. Yu. I. Petrov, *Clusters and Small Particles* [in Russian], Nauka, Moscow (1986).
24. A. B. Lebedev and A. A. Sorokin, "Numerical modeling of two-phase turbulent isobaric jets with homogeneous and heterogeneous condensation," *Trudy TsIAM*, No. 1288, 83–109 (1991).
25. *Turbulent Mixing of Gas Jets* (Ed. G. N. Abramovich) [in Russian], Nauka, Moscow (1974).